

DIRECT SELECTIVE LASER SINTERING OF TOOL STEEL POWDERS TO HIGH DENSITY: PART B – THE EFFECT ON MICROSTRUCTURAL EVOLUTION

S Akhtar*, CS Wright* and M Youseffi*

*Engineering Materials Research Group, University of Bradford, Bradford, UK

C Hauser[#], THC Childs[#], CM Taylor[#] and M Baddrossamay[#]
[#]School Of Mechanical Engineering, University of Leeds, UK

J Xie⁺ and P Fox⁺ and W O'Neill⁺

⁺Department of Engineering, University of Liverpool, UK

Abstract

This paper describes recent progress on the Direct Selective Laser Sintering of M2 [Fe-6W-5Mo-4Cr-2V-0.8C] high speed steel (HSS) and H13 [Fe-5Cr-1V-1Si-1.5Mo-0.4C] tool steel powders. Part B will focus on the microstructural evolution of laser scanned powder beds. It has been found that H13 powders are more amenable to Direct Selective Laser Sintering than M2 powders. Densities up to 90% are possible with H13 powder compared with 70% for M2. The relationship between alloy composition, microstructure, post-scanned density and scan conditions will be discussed for single track, single layer and multi-layer constructions.

Introduction

Selective laser sintering (SLS) is one of the more important solid freeform manufacturing processes developed in the last 10-15 years [1]. One of the main applications of SLS is for the manufacture of prototype or low volume production tooling using steel powders. Commercial systems are available which generate parts from either polymer coated steel powders [DTM RapidTool 2.0TM] or by processing a mixture of metal powders that contains a low melting point component [EOS DirectToolTM]. The need to post process, i.e. infiltrate with bronze, or the reliance on a low melting point liquid, leads to components with poor mechanical and tribological properties. This has led to a number of studies aimed to investigating Direct Selective Laser Sintering (DSLS) pre-alloyed metal powders with the aim of eliminating the above disadvantages. These studies generally made use of commercially available powder stainless steel [2, 3], and tool steels [4, 5]. Recently Dewidar [6] has reported studies on an experimental Mo-based High Speed Steel, a composition developed by Wright *et al.*[7], specifically as a “process-friendly” grade for processing by conventional die pressing and vacuum sintering. Whilst it is possible to process Stainless Steel powders to densities of +99% [3], less success has so far been achieved with tool steels. This paper presents results of investigations into the melting / densification behaviour of tool steel powders during DSLS which has the aim of identifying the factors which control the ability to fabricate fully dense, multi-layer components.

Experimental Techniques

Three types of powder were used in this investigation. Annealed water atomised M2 (WA-M2), gas atomised M2 (GA-M2) and gas atomised H13 (GA-H13). The water atomised M2 was sourced from Powdrex, UK and the gas-atomised powders were obtained from Osprey Metals Ltd, UK. The various size fractions used, along with Apparent Density and flowability (Hall Flowmeter) data are given in Table 1.

Powder Type	Size Fraction (μm)	Apparent Density (gcm^{-3})	Flowability (s/50g)
WA-M2	<150/+75	2.14	55.4
	<75/+38	2.18	59.8
	<38	2.60	No flow
GA-M2	150/+75	3.97	23.7
	<75/+38	ND	ND
	<38<	4.31	No flow
GA-H13	<150/+75	4.17	20.2
	<22	3.41	no flow

Table 1. Powder Properties of materials investigated

Selective laser sintering was performed on specially constructed machines at the Universities of Leeds and Liverpool. The Leeds machine includes a 250W continuous wave (CW) CO₂ laser. Preliminary studies were conducted at a Beam size of 1.1mm diameter. This was subsequently reduced to 0.55mm diameter. Galvanometer controlled mirrors direct the laser beam within a 70.0mm diameter build area which is housed in a 300 cm³ (L = 460mm, H = 260mm, and D = 250mm) chamber capable of sustaining a variety of atmosphere conditions including an absolute pressure of 10mbar. Details of this machine are given in Reference 2. In this study, the atmosphere inside the chamber was high purity argon (bottled argon at 99.9% purity). The chamber was evacuated to 30 mbar followed by a 15 min pre-sinter purge with argon at atmospheric pressure. During sintering the gas pressure inside the chamber was 30mbar above atmospheric. The Liverpool system, described by Morgan, et. al. [3], consists of a Rofin Sinar 90W, flash lamp pumped Q-Swiched Nd : YAG laser. An analogue galvanometer-scanning head attains beam position over an area of 80 x 80 mm². Pulse repetition rates are in the range 0 – 60kHz and minimum beam diameter is 80 μm . The shroud gas was nitrogen

The two systems employed different approaches to placing layers of powder. In the Leeds machine, the initial powder layer comprised loose powder to a depth of 5 mm contained in a mild steel tray. This layer was levelled with a blade to ensure a flat powder surface. Subsequent layers were deposited using a hopper system. The layer depth was 0.4 mm. In the Liverpool machine mild steel sheet was used as a substrate. In this system, the powder delivery system, which employs a counter rotating roller system [3], was optimised for an even 100 μm coating of powder to be layered for every build layer. Whilst all size fractions studied could be processed on the Leeds machine, the Liverpool machine was restricted to processing just the <38 μm and <22 μm fractions.

After sintering samples were prepared for metallographic examination by mounting and grinding on SiC paper to 1200 grit, then polished on cloths impregnated with 6 and 1 μm diamond. Polishing was completed using 0.05 μm γ -alumina. Samples were studied in the etched and un-etched conditions. M2 samples were etched in 5% Nital whilst 10% Nital was used for the H13 specimens. Samples were examined using both optical and scanning electron microscopy techniques.

Isopleths were calculated for the M2 and H13 systems using ThermoCalcTM [www.thermocalc.se] software and the SGTE SSOL database in order aid with both the selection of post-processing conditions and interpretation of microstructures, Figure 1.

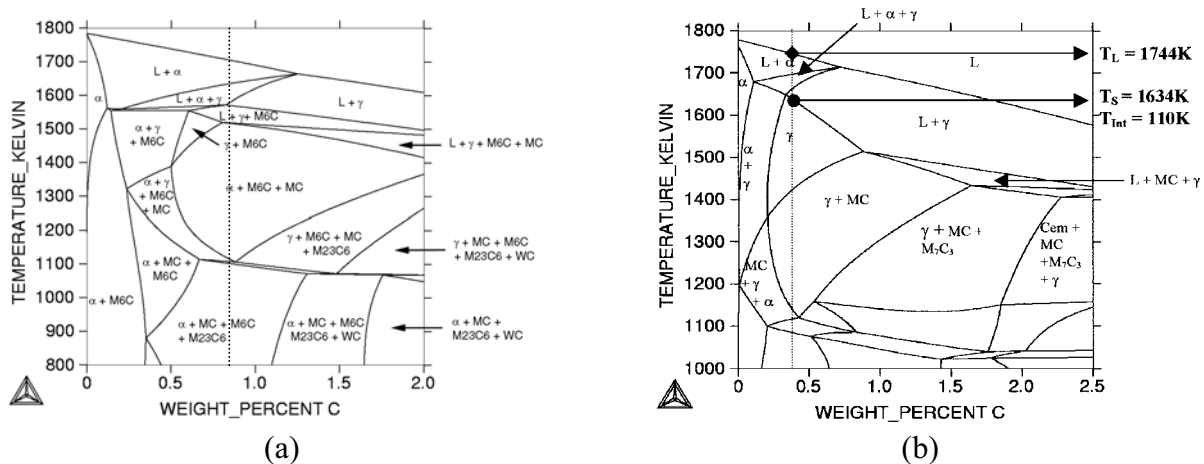


Figure 1. Calculated Isopleths for (a) Fe-6W-5Mo-4Cr-2V-C, and (b) Fe-5Cr-1V-1Si-1.5Mo-C systems

Results and Discussion

M2 Powders

Typical SEM micrographs of the “as-received” powders are given in Figure 2.

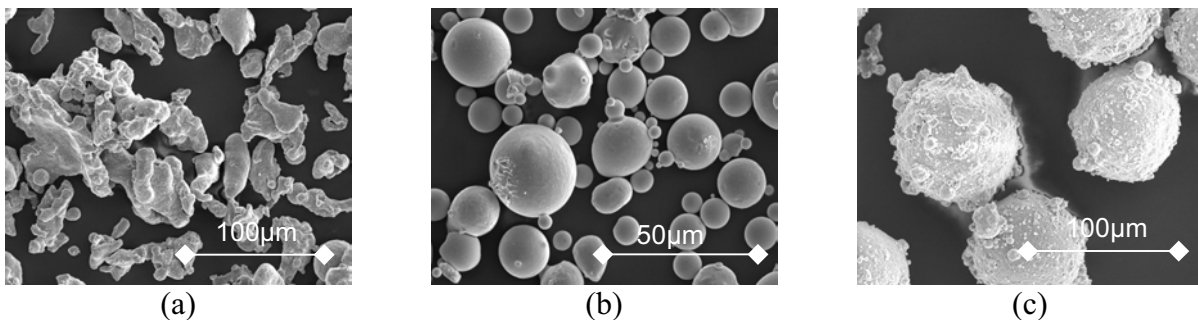


Figure 2. SEM micrographs of M2 powders. (a) WA-M2 <150 μm , (b) GA-M2 <38 μm , (c) GA-M2 <150/+75 μm size fractions.

The water-atomised powder was composed of highly irregular particles and, as such, is typical of this method of powder production. As expected the gas-atomised powders were composed of spherical particles. However, whilst the >38 μm GA-M2 size fraction consisted of

spherical particles with smooth surfaces [Figure 2(b)] the particle surfaces of the coarser fractions were much rougher due to the presence of many smaller satellites formed as a result of collisions during atomisation, Figure 2(c).



Figure 3 Microstructures of M2 powders. (a) Gas atomised $<150/+75$. Note the fine carbide network. (b) Water atomised $<38\mu\text{m}$ fraction. Note fine discrete carbides.

At the outset of this work two strategies were envisaged for the manufacture of high density, multi-layer components;

(a) Partial melting of successive powder layers forming sufficient liquid to bond both powders and layers together, followed by a post processing sintering step. High Speed steels are one of the few alloys systems that are commercially sintered to full density (i.e. +99% relative density) via a supersolidus liquid phase sintering mechanism [7]. The aim of the post processing step would be to vacuum sinter the laser sintered performs at a temperature of $\sim 1260^{\circ}\text{C}$, the optimum sintering temperature for conventional die-pressed M2 powders [10], initiate controlled re-melting, inducing densification through particle rearrangement and solution – re-precipitation mechanisms [7]. The challenge was to produce intact laser sintered performs which, in order to avoid distortion during post-processing sintering, contained uniform distributions of porosity

(b) Complete re-melting of powder layers.

The heating and melting behaviour of each batch of M2 powder was systematically studied using the CO_2 laser SLS machine at Leeds in order to identify appropriate processing conditions to achieve the two processing strategies. Single tracks were produced for a wide range of Laser power and scanning conditions. In common with previous investigations [2, 6] the results for M2 are presented as process maps, Figure 4.

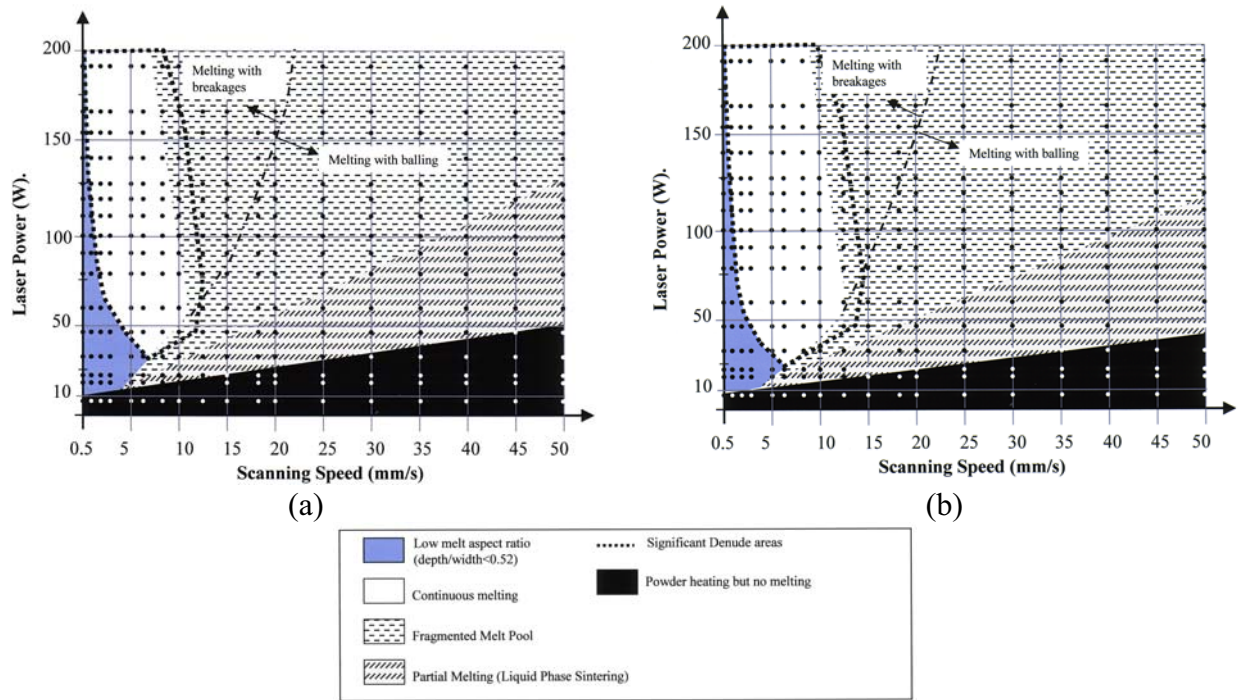


Figure 4. CW CO₂ laser process maps for gas-atomised M2 <150/+75µm fraction (a) 1.1mm and (b) 0.55mm spot size.

A feature of the process maps was that the size of the regimes and the positions of the boundaries defining each regime were comparable, irrespective of whether the powder was gas or water atomised and size fraction. Reducing spot size had a only small effect on increasing the size of the continuous melting regime, e.g. Figures 4(a) and 4(b). Attempts were made to fabricate single and multi-layer blocks (12 x 12 x 12 mm³) using conditions located within the partial melting and continuous melting regimes using the CO₂ laser SLS machine, Table 2.

Size Fraction (µm)	Beam Overlap (%)	Power (W)	Scan Speed (mms ⁻¹)	Spot Size (mm)	Comments
<38 _{water atomised}	25	60	60, 100	1.1	Single Layer
<38 _{gas atomised}	25	50,100	70,130	1.1	Single Layer
<75/+38 _{water atomised}	25	50,100	70, 130	1.1	Single Layer
<150/+75 _{gas atomised}	25	50, 60	100,130	1.1	Single Layer
<150/+75 _{gas atomised}	25	130, 135	8	0.55	Multiple Layer
<75/+38 _{gas atomised}	25,75	130	5,8	0.55	Multiple Layer
<75/+38 _{water atomised}	25,50,75	130	5,8,10	0.55	Multiple Layer

Table 2. Conditions used to process M2 powders using CW CO₂ Laser

Irrespective of powder type or particle size fraction, attempts to produce multi-layer blocks were unsuccessful using conditions located within the partial melting regime were unsuccessful. The sub 38µm water and gas atomised size fractions were difficult to spread, layers tended to form

furrows. However the major issue with processing within the partial melting regime was that at the conditions studied, insufficient melting took place to bond the next layer on to the previous layer, making it impossible to build intact blocks. Thus it was not possible to pursue fabrication of multi-layer components for M2 via strategy (a). Multi-layer blocks made from 25 individual layers were fabricated using conditions within the continuous melting regime. Unfortunately, the resultant blocks were very porous.

Using the Liverpool SLS system, it was possible to scan at up to 500 mms^{-1} and operate either in pulsed or continuous modes. Initial experiments were performed using water atomised M2 at scan speeds of $10 - 500 \text{ mms}^{-1}$, laser current 16-20A, Spot size = 0.1 mm, Beam overlap of 25-80%, pulse repetition frequency of 0kHz. The layer thickness was $100 \mu\text{m}$. Both single and 3 layer samples were produced. A feature of the scanned areas, though, was that they contained large amounts of un-melted powder. Removal of this by ultrasonic cleaning revealed that the beds were very porous, Figure 5(a). The porosity levels were unaffected by scanning conditions. This high level of porosity was attributed to the low apparent density of the water atomised powder arising from its highly irregular shape, Table 1, and the layer thickness. In previous studies with 316L stainless steel, operating in pulsing mode blocks with 100% relative density being obtained [4]. Consequently, additional experiments with M2 powders were carried out at layer thickness of 100 and $50 \mu\text{m}$, pulse repetition frequencies of 40 and 50kHz, scan speed = 500 mms^{-1} , current = 20A, spot size = $100 \mu\text{m}$, beam overlap = 50%. Blocks $5 \times 15 \times 15 \text{ mm}^3$ were produced. Operating in pulse repetition mode resulted in an increase in density compared to continuous mode. However densities were only 5.5 gcm^{-3} , i.e. $\sim 70\%$ relative, and were independent of processing conditions, Figure 5(b).

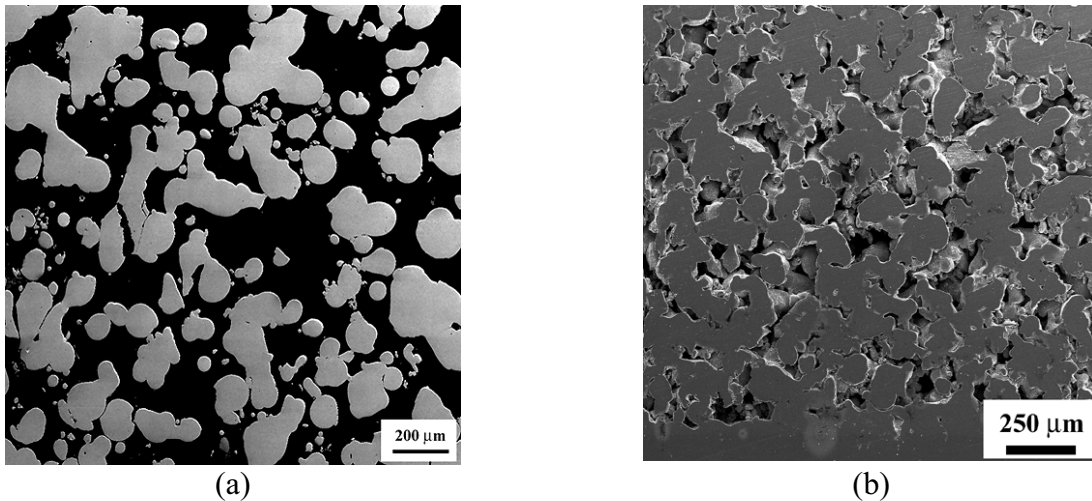


Figure 5. Micrographs of Nd : YAG laser scanned multi-layer M2 (a) $<38 \mu\text{m}$ WA-M2, 400 mms^{-1} scan speed, 50% beam overlap, current 20A, spot size 0.1mm, (b) 500 mms^{-1} scan speed, 50% beam overlap, current 20A, spot size 0.1mm, pulse rate 40kHz. ($100 \mu\text{m}$ layer thickness).

Despite the higher apparent density of the $<38 \mu\text{m}$ gas atomised powder, Table 1, use of this powder had no beneficial effects on the density of laser scanned blocks, densities were similar to those obtained for $<38 \mu\text{m}$ water atomised M2 powder.

The microstructures of samples produced on the two systems were comparable and independent of starting powder. Single layers produced using the CO₂ laser operating within the partial melting regime contained regions of un-melted powder, Figure 6(a). The melted regions had a very fine cellular - dendritic structure (grain size <10µm) with fine eutectic networks at grain boundaries, Figure 6(b). Partially melted regions were also visible [Figure 6(c)].

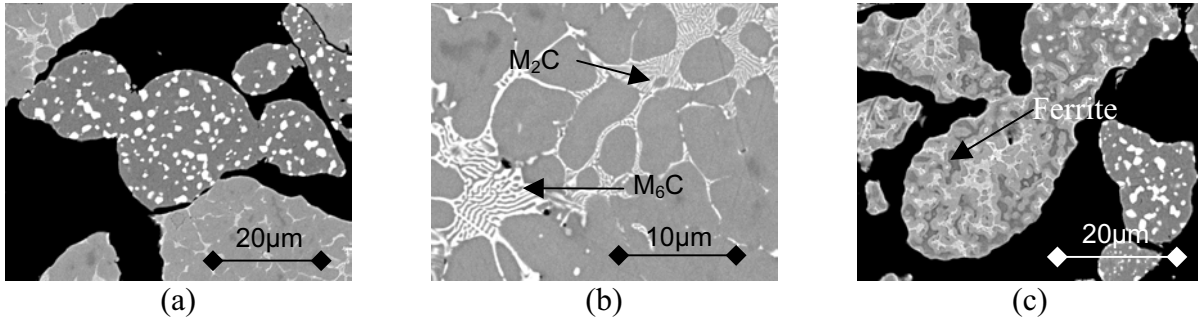


Figure 6 CW CO₂ M2 single layers at 1.1mm spot size. (a) <38µm, 60W, 25% beam overlap, 100mms⁻¹ Scan speed, (b) <38µm, 60W, beam overlap 25%, scan speed 70mms⁻¹, (c) <38µm, 60W, beam overlap 25%, scan speed 100mms⁻¹.

The dark areas [Figure 6(c)] are believed to be ferrite, suggesting that these regions been reheated to within the L + γ + α or L + γ region of Figure 1(a). Two types of eutectic were observed. Given the small size of the eutectics it was not possible to identify them using X-ray microanalysis. However based on both grey levels in Back Scattered Electron imaging (Atomic Number contrast) and eutectic morphology, it is possible to identify the carbide components as M₆C (Fe-W-Mo rich) and M₂C (Mo-W-Fe-V rich) [8]. Irrespective of composition or cooling rate, M₆C adopts a characteristic “herringbone” structure. The presence of M₂C is not expected from Figure 1(a), instead V rich MC would be expected to form under equilibrium cooling. High cooling rates, such as those of laser processing techniques, favour M₂C formation over MC [8]. M₂C eutectic can adopt one of three morphologies, feathery, cellular or lamellar [8]. High cooling rate also favours the formation the cellular morphology observed in the SLS samples [8]. Microstructures of single layer samples processed in the continuous melting regime were comparable, the only difference being a reduction in the amount of un-melted powder present.

Examination of the multi-layer samples revealed that re-melting was taking place to a depth of 2-3 layers. For example in the blocks produced from 25 powder layers on the CO₂ laser system only 13 layers were visible afterwards. In terms of eutectic type and morphology, presence of partially melted regions, the microstructures were identical to the single layer samples. However an important additional microstructural feature was the presence of coarse eutectic layers within the blocks, e.g. Figure 7(a), believed to be formed by epitaxial solidification at solid-liquid interfaces.



Figure 7 Micrographs of M2 CW CO₂ laser multi-layer specimens (a) GA-M2 <150μm<38μm, 60W, 25% beam overlap, 70mms⁻¹ Scan speed, 0.55 mm spot size (b) Post processed sample – 1260°C for 60 min.

Eutectic structures in High Speed Steels are considered to be detrimental to mechanical properties. Hoyle [9] demonstrated for conventional cast HSS that it was possible to refine the “as cast” eutectic structures by reheating to just above the solidus followed by slow cooling. In a similar manner, the multi-layer blocks were subjected to a post processing step which involved heating in vacuum at 10°Cmin⁻¹ to 1260°C, the optimum Supersolidus Liquid Phase Sintering temperature for M2 powders [10], holding for 60min then furnace cooling at an average rate of ~2°Cmin⁻¹ to room temperature. Whilst this treatment did not produce any further densification, it resulted in the breakdown of the eutectic structures; networks being replaced by fine, discrete carbides with regions such as those of Figure 7(a) being replaced by coarser carbide clusters, Figure 7(b). This is considered significant because even if M2 powders could be processed to ~100% density by DSLS, such regions would be potential points of weakness since it is known that in cast wrought and powder metallurgy processed HSS that carbide clusters are preferred sites for crack nucleation at low applied stresses under static and dynamic loading [11].

H13 Powders

The Gas atomised H13 powders were spherical with minimal satellites. The microstructure of “as-received” powders comprised cellular-dendritic grain structure with continuous grain boundary carbide films, Figure 8. The grain size decreased with particle size.



Figure 8. Microstructure of gas atomised H13 <150/+75μm size fraction

Figure 9 shows the Process Map for <150/+75μm powder processed using a 0.55mm spot size on the CWCO₂ system.

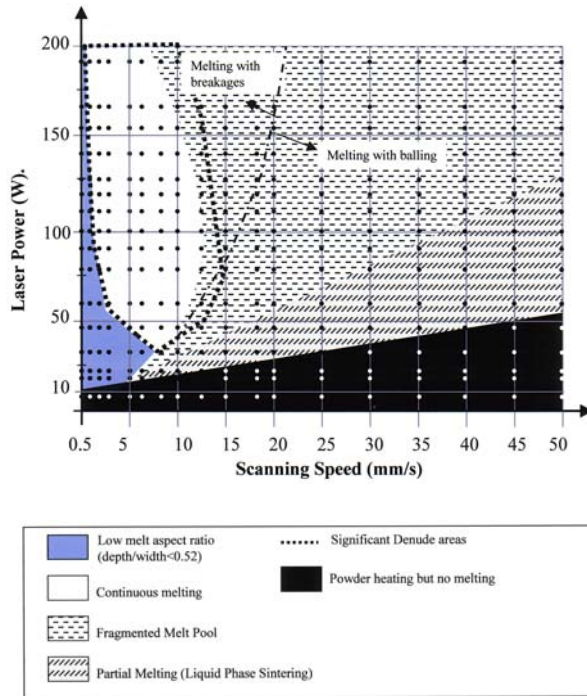
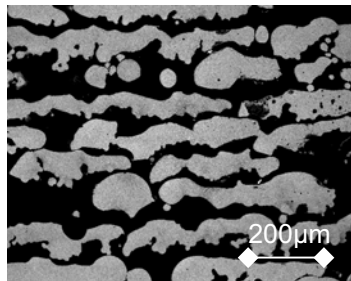


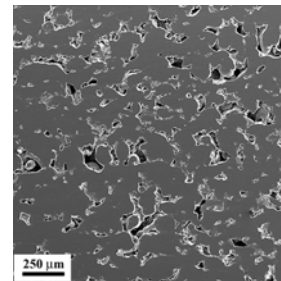
Figure 9. CW CO₂ laser process maps for gas-atomised H13 <150/+75 μm fraction, 0.55mm spot size

Comparing Figure 9 with Figure 4(b), it can be seen that the process map for H13 is comparable to those for M2 powders. Interestingly, processing H13 powders within the partial melting regime of Figure 9 was slightly more successful than with M2 in that it was possible to produce multi-layer blocks. The individual layers were ~1/3 thinner than for M2 processed in the same regime but these multi-layer blocks were very porous and fragile, Figure 10(a).

Much more promising results were obtained with H13 compared to M2 in the Nd : YAG SLS. Processing at condition of Pulse repetition frequency of 30kHz, scan speed 500mms⁻¹, current 20A, spot size 100μm, beam overlap 50% give well-bonded, multi-layer blocks with a density of 90%, cf. Figure 10(b) and Figure 5(b).



(a) <150/+75μm size fraction



(b) <22μm size fraction

Figure 10. H13 multi-layer samples (a) CW CO₂ laser at 0.55mm Spot size size, 5mms⁻¹ scan speed, 50% Scan spacing, 32W Power. (b) Nd : YAG laser at 500 mms⁻¹ scan speed, 50% beam overlap, current 20A, spot size 0.1mm, pulse rate 30kHz. (100μm layer thickness)

Figure 11 shows typical microstructures produced for continuous melting using the Nd: YAG system and partial melting using the CO₂ system.

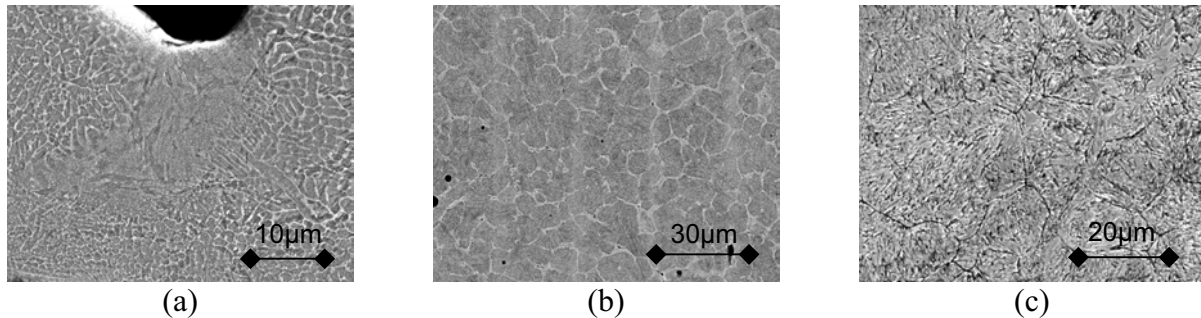


Figure 11. Micrographs of H13 powders scanned at same conditions as Figure 10. (a) Nd : YAG laser [Pulsed Mode], (b) and (c) CW CO₂ laser

Processing using the Nd : YAG laser produced a fine, grained cellular – dendritic size with continuous grain boundary carbide films, Figure 11(a). The matrix was martensitic. Carbide depleted zones were observed [Figure 11(a)] and in some areas there was no bonding between layers. Due to the fineness of the microstructure, this carbide phase could not be identified using X-ray microanalysis. However, unlike M2, coarse carbide clusters were not observed at interfaces. Superficially the microstructures of the samples produced by processing in the partial melting regime of the CO₂ laser were similar to those produced by Nd : YAG laser scanning. They appeared to consist of a cellular – dendritic grain structure, a martensitic matrix and continuous grain boundary carbide films, Figure 11(b) and (c). Detailed observation using SEM revealed a more complex situation in that the network features were simply regions of differential contrast, they were crossed by austenite grain boundaries and by individual martensite laths, Figure 11(c). X-ray microanalysis indicated that these regions were slightly richer in Chromium than the grain interiors. This type of structure could arise due to reheating of a previous solidified layer during subsequent scanning of the top layer of powder. The carbides present in laser scanned H13 materials have yet to be positively identified but it can be inferred from Figure 1(b) that non-equilibrium solidification will result in the formation of Cr rich M₇C₃ carbide in preference to vanadium-rich MC predicted for equilibrium solidification. M₇C₃ carbides readily dissolve in austenite at temperatures above ~950°C. Reheating for a short time, at a temperature below the solidus sufficient to dissolve the carbides, yet high enough to form austenite, followed by rapid cooling could, in principal, produce the microstructure seen in Figure 11(c). Carbon diffusion rates are much high in γ -Fe than Chromium diffusion rates and, if the time at temperature is insufficient for homogenisation, a coring effect will result, as indicated by X-ray microanalysis. Once the carbides have dissolved there will be no pinning effect and an austenite grain structure will form with grain boundaries cutting across the cored regions. The austenite will transform to martensite on cooling with individual laths passing through cored regions. It is not yet understood why this structure was not observed in the Nd : YAG processed powders.

The results presented here indicate, as with the previous studies of Nui and Chang [4, 5], that gas-atomised powders are more suited to the DSLS approach than water-atomised powders. Whether this is due to the higher oxygen content of water-atomised powders, as suggested by them or particle morphology have still to be established. For example, are the differences in

behaviour due to lower apparent density of water atomised producing less dense powder beds or is due to the bed powder flowability and how the powder interacts and flows into the moving melt pool. More interestingly, the current studies have shown that H13 powders are more amenable to DSLS than M2 powders. Given that powder properties for the two compositions are comparable this would suggest that alloy composition has an important role to play, particularly since similar sized stainless steel powders can be processed to 100% density [3]. The reasons for this are the subject of ongoing investigations.

Conclusions

[1] M2 high speed steel powders are not amenable to processing to full density by a DSLS processing. The maximum density achieved in multi-layer samples, using pulsed Nd : YAG processing was only 70% relative. Much lower densities were obtained using CW CO₂ and CW Nd : YAG processing operating in the same continuous melting regimes.

[2] Gas-atomised H13 powders are amenable DSLS with densities of 90% relative being achieved using pulsed Nd : YAG processing operating in a regime of continuous melting

[3] The reasons for the differences in processing behaviours of M2 and H13 powders of similar powders properties are, as yet, unclear.

Acknowledgements

The research reported in this paper is a joint project between the Universities of Bradford, Leeds and Liverpool, funded by the UK Engineering and Physical Sciences Research Council under Grant Number GR/R32222.

References

- [1] KW Dalgarno and CS Wright; "Approaches to Processing Metal and Ceramics through the Laser Scanning of Powder Beds", *Society of Manufacturing Engineers*, Technical Paper PE03-143, 2003.
- [2] C Hauser, THC Childs & KW Dalgarno, "Selective Laser Sintering of Stainless Steel 314HC Processed Using Room Temperature Powder Beds", *proc. Solid Freeform Fabrication Symposium* Austin, Texas August 9 – 11, 1999, pp273-280.
- [3] RH Morgan AJ Papworth, C Sutcliffe, P Fox & W O'Neill, "High Density Net Shape Components by Direct Laser Re-melting of Single Phase Powders", *J Materials Science*, 2002, **37**, 3093-3100.
- [4] NJ Niu and ITH Chang, "Selective Laser Sintering of Gas and Water Atomised High Speed Steel Powders", *Scripta Materialia*, 1999, **41**, pp 25 – 30.
- [5] NJ Niu and ITH Chang, "Instability of Scan Tracks of Selective Laser Sintering of High Speed Steel Powder", *Scripta Materialia*, 1999, **41**, pp 1229 – 1234.
- [6] MM Dewidar, "Direct and Indirect Laser Sintering of Metals" *PhD Thesis*, University of Leeds, 2002.
- [7] CS Wright et. al., "Supersolidus Liquid Phase Sintering of High Speed Steels – Part 3 the Computer Aided Design of Sinterable Alloys", *Powder Metallurgy*, 1999, **42**(2), pp 131-145.

- [8] M Boccalini and H Goldenstein, "Solidification of High Speed Steel", *International Materials Reviews*, 2001, **46**(2) pp 92 –115.
- [9] G Hoyle, "Modification of the Cast Structure of High Speed Steel", *J.Iron Steel Institute*, 1959, November, pp254-269.
- [10] CS Wright and B Ogël, "Supersolidus sintering of high speed steels. Part I-supersolidus sintering of molybdenum based alloys", *Powder Metallurgy*, 1993, **33**(3), pp 213-219.
- [11] MA Gomes, AS Wronski and CS Wright, "Fracture behaviour of a highly alloyed high speed steel", *Fracture and Fatigue of Engineering Materials and Structures*, 1995, **18**, pp 1 -18